JGR Space Physics

RESEARCH ARTICLE
10.1029/2019JA026480

Perturbations of O(^{1}D) VER, Temperature, Winds, Atomic Oxygen, and TEC at High Southern Latitudes

Marianna Shepherd[1], **Gordon Shepherd**[1], **and Mihail Codrescu**[2]

[1]Centre for Research in Earth and Space Science, York University, Toronto, Ontario, Canada, [2]Space Weather Prediction Center, NCEP, NOAA, Boulder, CO, USA

Key Points:
- Previously unrecognized perturbations in thermospheric and ionospheric winds are observed at a specific high latitude location, 50°E–150°E and at 50°S–70°S
- The neutral winds show a reversal to westward reaching −450 m/s, with a peak and trough structure of meridional wind, having an eastern boundary at ~150°E
- Enhancements occur in daytime O(^{1}D) emission, temperature, and TEC; atomic oxygen is depleted

Correspondence to:
M. Shepherd,
mshepher@yorku.ca

Citation:
Shepherd, M., Shepherd, G., & Codrescu, M. (2019). Perturbations of O(^{1}D) VER, temperature, winds, atomic oxygen, and TEC at high southern latitudes. *Journal of Geophysical Research: Space Physics*, *124*, 4773–4795. https://doi.org/10.1029/2019JA026480

Received 8 JAN 2019
Accepted 22 MAY 2019
Accepted article online 6 JUN 2019
Published online 25 JUN 2019

Abstract The study investigates previously unrecognized wind reversals of the daytime thermosphere in the Southern Hemisphere at latitudes of 50°S–70°S employing observations of O(^{1}D) airglow volume emission rates (VER), temperature, and neutral winds at 170–300-km height by the Wind Imaging Interferometer. Atomic oxygen densities derived from the Wind Imaging Interferometer O^+ (732–733 nm) emission observations were also considered together with contemporaneous observations of total electron content by the TOPEX Poseidon satellite mission. The O(^{1}D) VER for fall equinox (March/April 1994) and summer solstice (January 1995) revealed a peak in the VER over the longitude range of 50°E–150°E, for both seasons and daytime local times. The Doppler temperatures also exhibited a maximum at the same location and times. The co-located zonal wind field shows a westward trough at 50°E–150°E with wind speeds reaching −450 m/s and an eastward peak at 200°E–300°E. Meridional winds show a "peak and trough" structure over the 50°E–150°E region, with a distinct eastern boundary at ~150°E. During summer solstice the atomic oxygen is depleted at the region of the O(^{1}D) VER enhancement in the presence of westward zonal wind. However, the total electron content observations showed a peak that coincided with the O(^{1}D) VER and temperature enhancements.

Plain Language Summary The study investigates unusual perturbations in upper atmospheric winds that occur at a very specific location in the high-latitude Southern Hemisphere. These include wind reversals, enhancements in the "red line" atomic oxygen airglow emission at 630.0 nm, temperature, depletion of atomic oxygen, and enhancements of ionospheric electron density. The location is 50°E–150°E longitude, 50°S–70°S latitude. The atmospheric observations were made by the Wind Imaging Interferometer, launched on NASA's Upper Atmosphere Research Satellite in 1991; these continued until 2003. The wind reversals involved westward winds of as strong as 450 m/s. The electron densities were of total electron content integrated along the line of sight from the satellite to the Earth and were obtained from the TOPEX satellite for the same time periods as the Wind Imaging Interferometer observations. Measurements were made at equinox and summer solstice and the atmospheric observations were the same for both. These new observations point the way to future studies of this highly localized phenomenon.

1. Introduction

There have been extensive studies of neutral thermospheric dynamics at high latitudes but more remains to be explored, in part because of the lack of observations. Richmond et al. (2003) investigated high-latitude winds observed with the Wind Imaging Interferometer (WINDII) on the Upper Atmosphere Research Satellite (UARS), finding winds exceeding 300 m/s, and found a well-defined correlation with the interplanetary magnetic field, in particular the B_y and B_z components. Thayer et al. (1995) investigated ion and neutral winds observed from Thule, Greenland at 77.5°N geographic latitude and found during disturbed conditions antisunward ion winds reaching 1,000 m/s, with neutral winds reaching 500 m/s. Wind data from many sources were combined by Dhadly et al. (2017) to generate neutral wind maps for quiet conditions for different seasons. A second study by Dhadly et al. (2018) provided the same for disturbed conditions. Those presentations were polar projections of magnetic latitude versus magnetic local time but did not contain any longitude information.

It was recently found that when daily high-latitude WINDII wind data were plotted as a function of altitude versus geographic longitude by Shepherd and Shepherd (2018) that highly localized zonal wind reversals from eastward to westward frequently occurred, with very strong westward winds, 450 m/s and greater. These always appeared at the same longitudes, 100°–200°, in the Southern Hemisphere and 280° to 360°

in the Northern Hemisphere, at the same latitudes of 60°–70° in both hemispheres. These preliminary wind observations were derived from Doppler shifts of the O(^{1}S) green line of atomic oxygen at 557.7 nm and the authors suggested the name "wind wall" for this sharp reversal.

The present study extends those first unique observations by making use of the O(^{1}D) red line of atomic oxygen at 630 nm, which occurs at higher altitude and from which Doppler temperatures can also be obtained. Because the altitude of interest for the UARS mission as a whole did not extend above 120 km these data were taken less frequently than for other emissions but for this study it was possible to find data for two Southern Hemisphere seasons, summer solstice and fall equinox. Contemporaneous total electron content (TEC) data from the TOPEX Poseidon satellite were also included in the study, providing more information about this phenomenon.

A precursory aspect of this phenomenon is atmospheric composition. G. Shepherd and Cho (2017) investigated atomic oxygen concentrations obtained from WINDII measurements of $O^+(^2P)$ emission at 730 nm. With observations extending poleward only to 40°S latitude they found a depletion in atomic oxygen concentration at the same longitudes at which the wind wall was later found at high latitudes. The same depletion, also extending to 40°S latitude, was seen in NRLMSIS model results and in the Global Ultraviolet Imager $[O]/[N_2]$ data from the TIMED (Thermosphere, Ionosphere, Mesosphere Energetics and Dynamics) satellite. There was an even earlier precursor to the observation of the atomic oxygen depletion made by Laux and von Zahn (1979) with a gas analyzer on the Esro 4 satellite. They found N_2 and Ar enhancements, and O and He depletions that were in close proximity to the Magnetic Dip Poles. In the Southern Hemisphere the magnetic pole is at 64°S latitude and 125°E longitude, very close to the wind reversals and O depletion reported upon here. The present study is intended to describe the wind wall in more detail employing a larger body of observations of winds, temperature, TEC, and atomic oxygen concentration.

The paper is organized as follows: section 2 provides a brief description of the observations considered in the study. Results are presented in sections 3 and 4, followed by a discussion of some of the results obtained, summary and conclusions of these results, presented in sections 5 and 6, respectively.

2. Observations

The study employed observations from WINDII on UARS in the Southern Hemisphere for the period of fall equinox, March–April 1994, and summer, January 1995. The WINDII instrument, described in detail in G. Shepherd et al. (1993), was launched on September 1991 and continued operation until 2003 measuring five oxygen airglow emissions at the Earth's limb allowing measurements from 80- to 300-km altitude and providing extensive measurements of the thermosphere during day and night. Due to UARS's orbit inclination of 57° and WINDII's sideways viewing the latitude range of 42°S–42°N was viewed continuously, while high latitudes up to 72° were observed in alternate hemispheres for 36 days at a time. Over the course of a day the satellite normally completed 15 orbits as the Earth rotated beneath it. Therefore, distinct local times are sampled at a given latitude for both ascending and descending nodes of the orbit. The local time on each day appears 20 min earlier than that of the day before; thus, 36 days are required to sample a full 24-hr period.

The atomic oxygen O(^{1}D) airglow, Doppler temperatures, neutral winds (zonal and meridional), and atomic oxygen densities are used to examine the daytime dynamical structure of the upper atmosphere at altitudes from 170 to 300 km. The thermospheric O(^{1}D) 630-nm airglow emission was chosen because of the information it could provide on the electron density and neutral winds in the *F* region of the ionosphere. This is in contrast to the earlier wind wall study by Shepherd and Shepherd (2018) which utilized the more frequently observed O(^{1}S) emission. Because this height region was entirely outside the scope of the UARS mission it was agreed that dedicated O(^{1}D) observations would be made one full day each week. Later the observation schedule was adjusted and O(^{1}D) airglow observations were carried out more frequently, particularly during 1993 and a few more days in 1994 in addition to the original one-day-per-week schedule. The Doppler temperature and neutral winds were retrieved from the O(^{1}D) emission rates. Various aspects of the retrieval of the O(^{1}D) airglow volume emission rates, neutral winds, and Doppler temperatures were discussed in G. Shepherd et al. (1993), Gault et al. (1996), and Lathuillère et al. (2002), and summarized by G. Shepherd et al. (2012). A brief summary with an emphasis on the O(^{1}D) observations and their accuracy was also

presented in M. Shepherd (2016, 2018). The O(^{1}D) measurements along the satellite track were separated by about 3° in latitude. The simultaneous observations of atomic oxygen O(^{1}D) airglow VER, zonal and meridional winds, and Doppler temperature used in the present study are for daytime at 50°S–70°S with solar zenith angles less than 96°. For this latitude range there were 51 days of O(^{1}D) airglow VER, Doppler temperature, and zonal and meridional wind observations between November 1991 and March 1995. The periods of 28 March to 10 April 1994 (day of year (DoY) 94,087–94,100) and 2–9 January 1995 (DoY 95,002–95,009) were chosen as they contain a number of consecutive or nearly consecutive (every other day) observations (DoY 94,087 means day 87 of 1994). The winds are retrieved by combining observations from WINDII's two fields of view where they overlapped, while the data for O(^{1}D) VER are from one field of view only.

In describing the results that follow and in particular those pertinent to the neutral winds the terms "peak/maximum" are used to describe the maximum eastward/northward (positive) directions of the zonal/meridional winds. Accordingly, a "trough/minimum" refers to westward/southward (negative) directions of the zonal/meridional winds.

Atomic oxygen plays an important role in the production of O(^{1}D) VER in daytime through photoelectron impact. Atomic oxygen [O] density values derived from the WINDII O^+ (^{2}P-^{2}D) 732- and 733-nm daytime airglow emissions by G. Shepherd et al. (2016) and G. Shepherd and Cho (2017) were also used in the study. For the O^+ 732-nm emission the excitation mechanism is solar photon ionization from the ground state of O. As G. Shepherd and Cho (2017) show the [O] can be determined from the solar flux if the quenching rates are known. All WINDII observations shown here are for daytime, covering the latitudinal range of 50°S–70°S from 170 to 300 km during fall equinox, 28 March to 10 April 1994, and summer solstice, 2–9 January 1995. From the existing [O] data set observations only for 3 and 7 January 1995 are within the O(^{1}D) periods considered in the present study.

In addition to the WINDII thermospheric observations, the study employed contemporaneous observations of TEC from the TOPEX Poseidon satellite experiment (Fu et al., 1994; Codrescu et al., 1999, 2001, and references therein). The satellite carried onboard a suite of instruments which included a dual-frequency altimeter that provided ionospheric corrections for the continuous sea height measurements over the oceans. These were differential group path defect measurements, from which TEC in TECU (1 TECU = 10^{16} e^- m^{-2}) was calculated. TOPEX TEC provides the integrated electron density extending from the satellite orbiting at 1,336 km to the subsatellite reflection point on the ocean's surface with an inclination of 66°. The TOPEX Poseidon covered the Earth in a 9.9156-day cycle with one complete cycle made of 254 descending and ascending passes. These 254 passes repeat exactly in subsequent 9.9156-day periods, while the orbit drifts westward by 2° (8 min in local time) per day, taking 90 days for a 24-hr period of local time to be sampled. Further information can be found in Codrescu et al. (1999, 2001). Daily TOPEX TEC observations for the same time period as WINDII are examined over the latitude range of 50°S–67°S. Both observations are presented in geographic coordinates. Because of the observation format, all observations during the 28 March to 10 April 1994 equinox period are for the period of ~7 LT–16 LT, while during the 2–9 January 1995 summer solstice period, the observations cover local times from ~22 LT to 7 LT. TOPEX TEC observations with local time coverage of 13.6 LT–15.6 LT and 18.3 LT–20.4 LT, during 2–12 February 1996, are also considered in this study.

All available data at 50°S–70°S (67°S) were separated depending on which part of the satellite orbit (ascending or descending) the data were obtained. This is necessary because at a given latitude band both WINDII and TOPEX sample two different local times during the ascending and descending parts of their orbits.

3. Results

3.1. O(^{1}D) Volume Emission Rates

The daytime red line O(^{1}D) emission is produced by three main mechanisms: (1) dissociative recombination of O_2^+ by electrons, (2) photoelectron impact on atomic oxygen, and (3) photodissociation of O_2 (Singh et al., 2010, and references therein).

Figure 1 shows the O(^{1}D) VER as a function of altitude and longitude for 50°S–70°S latitude over the altitude range from 170 to 290 km, for 28 March to 10 April 1994 (fall equinox). For brevity, only plots for every four

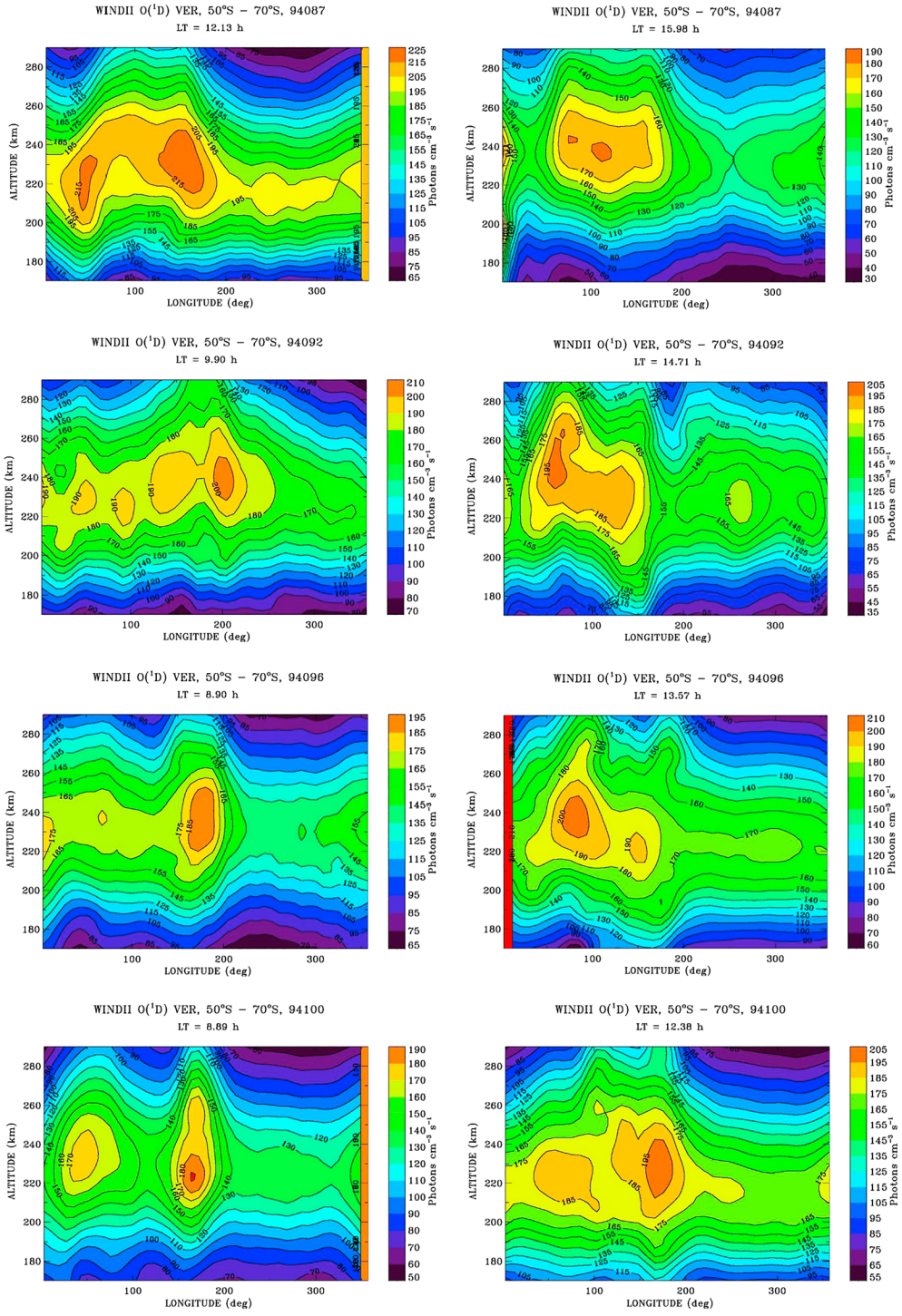

Figure 1. WINDII O(^{1}D) VERs at 50°S–70°S as a function of longitude and altitude for 28 March to 10 April 1994 (DoYs 94,087–94,100). Here and elsewhere, unless said otherwise, the left column shows observations from the descending part of the satellite orbit, while the right column presents observations from the ascending orbit.

days are shown, namely, 28 March (DoY 94,087), 2 April (DoY 94,092), 6 April (DoY 94,096), and 10 April (DoY 94,100). Here and elsewhere, unless said otherwise, the left column shows observations from the descending part of the satellite orbit, while the right column presents observations from the ascending part. The images proceed downward for successive days. The images cover a local time range from 8.9 LT

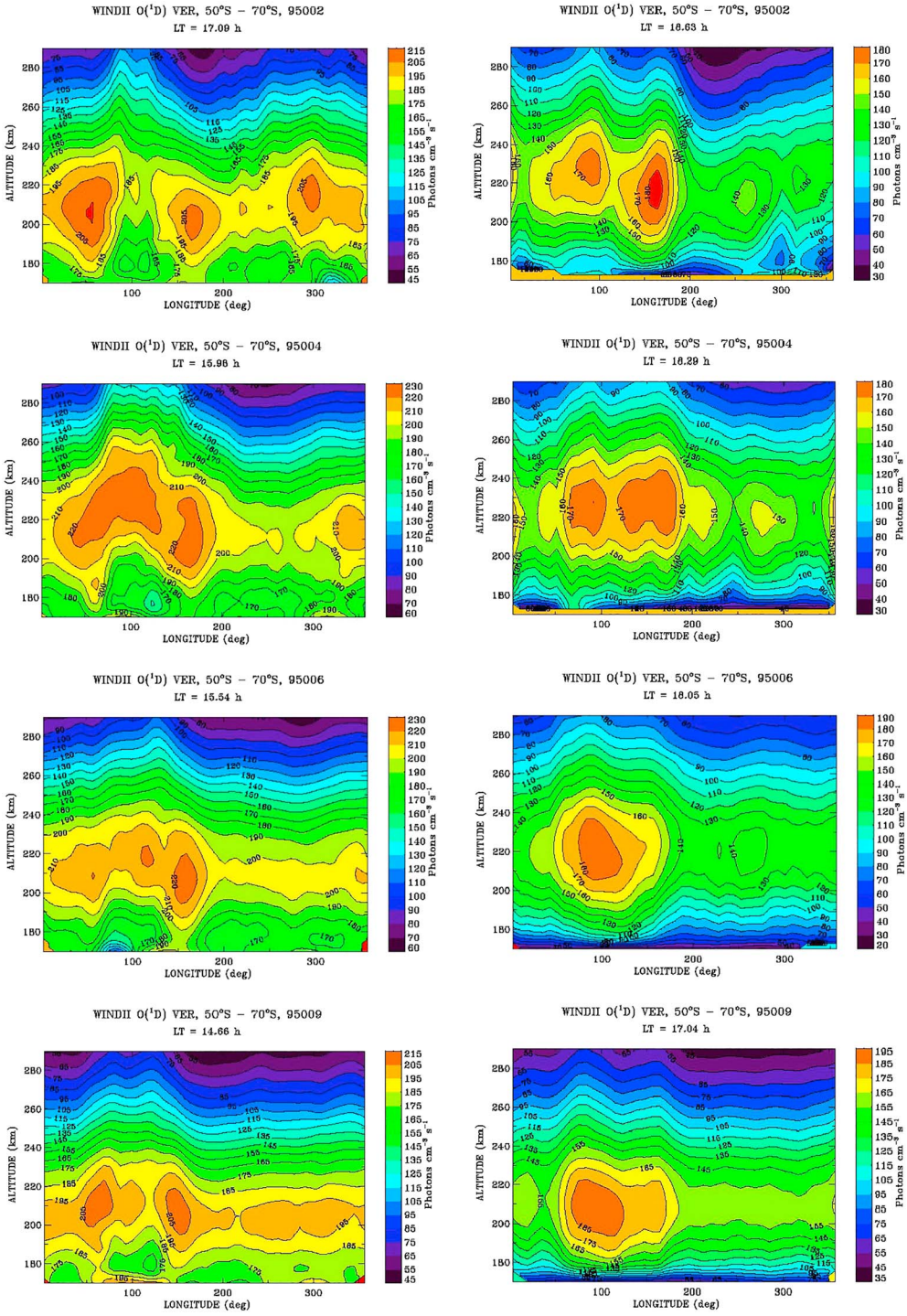

Figure 2. The same as in Figure 1 but for 2–9 January 1995 (DoYs 95,002–95,009).

to 16 LT. What is remarkable is that the O(^{1}D) VER shows a persistent enhancement between ~50°E and 200°E with a peak at ~170°E–200°E longitude and a second one at ~50°E. Over time the magnitude of the O(^{1}D) VER peaks varies, but their position remains within the 0°–200°E longitude range and is local time independent.

Figure 2 shows a similar pattern observed during the 2–9 January 1995 (DoY 95,002–95,009), summer solstice, also in the Southern Hemisphere. In spite of the fact that the January data cover a different local

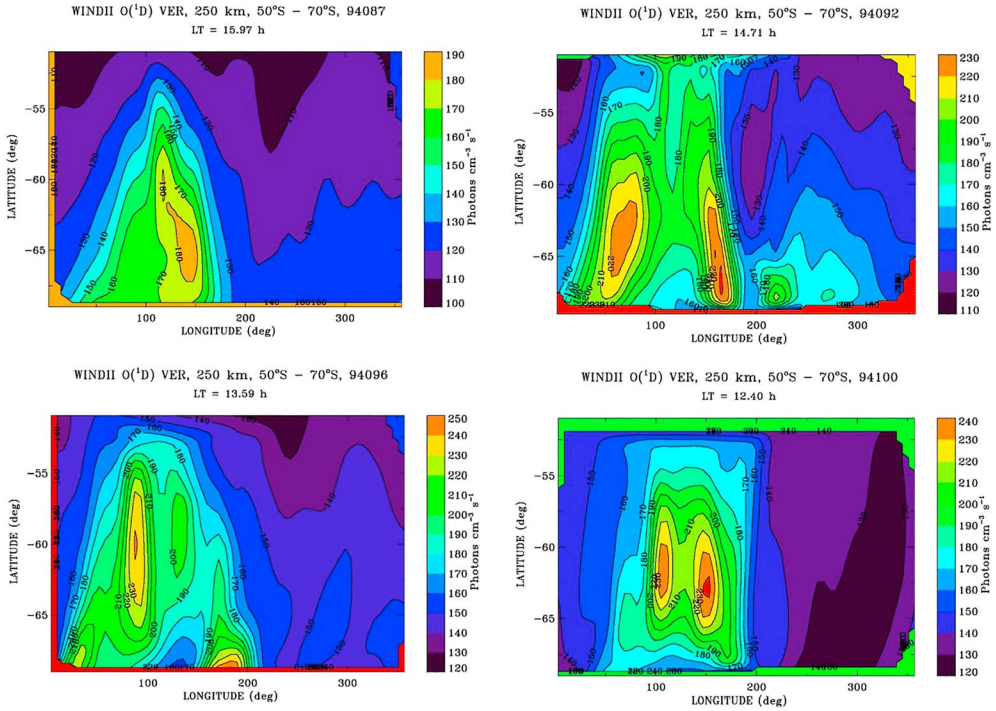

Figure 3. Maps of the O(^{1}D) VER at 250-km height and 50°S–70°S for 28 March to 10 April 1994 (DoYs 94,087–94,100) for the ascending part of the WINDII orbit.

time period, 14.7 LT to 18.6 LT from that for equinox, the O(^{1}D) VER enhancement between 50°S and 150°S–170°S remains very similar to that for equinox. The O(^{1}D) VER peak is within 50°E–150°E longitude, although on occasion accompanied by additional peaks. The altitude of the peak on average is lower in January 1995, at ~210–230 compared with 220–240 km for the March/April 1994 period. Maps of the O(^{1}D) VER at 250 km for 50°S–70°S given in Figure 3 show the latitude extent of the observed emission enhancements for the days presented in Figure 1. The O(^{1}D) enhancement extends through the latitude band but is confined to the longitude range from 0° to 200°E with peaks at ~50°E–100°E and 140°E–170°E and 60°S–65°S, especially for DoYs 94,092, 94,096, and 94,100; the rest of the field shows very low/depleted O(^{1}D) VER. The enhancement at 50°E–200°E and depletion at 200°E–360°E were also observed during the January 1995 period, not shown here for brevity.

3.2. Doppler Temperatures

The Doppler temperatures derived from the observed O(^{1}D) VER over the latitude range of 50°S–70°S and altitudes from 170 km to 290 are shown in Figure 4 for March/April 1994 and in Figure 5 for January 1995. The Doppler temperatures in March/April 1994 show peaks at ~50°E–200°E above 290 km for both the ascending and descending parts of the orbit, but their effect extends down to ~170-km height. The region of 200°E–360°E is colder, with a wave-1 pattern at these altitudes. An exception to this is DoY 94,092, 2 April 1994, of enhanced geomagnetic activity (Kp = 4.7–5.3, Ap = 39–56) with a second peak at 220°E (14.7 LT; Figure 4, right column, ascending part of the orbit). The scale for each plot reflects the range of the observed values on that day, in order to reveal better the signatures present. The Doppler temperatures in January 1995 descending observations (left column, Figure 5) show a similar pattern as those seen in March/April 1994, namely, a peak at ~70°E–100°E and cold upper atmosphere from ~150°E to 360°E. As the local time progresses toward the early evening hours (17 LT–18.6 LT), the region of temperature enhancement, centered around 100°E–150°E, becomes broader in its longitudinal extent. In summary, the Doppler temperatures show the same longitude variation as the O(^{1}D) VER suggesting downward motion, bringing warmer air and enhanced atomic oxygen density to lower levels.

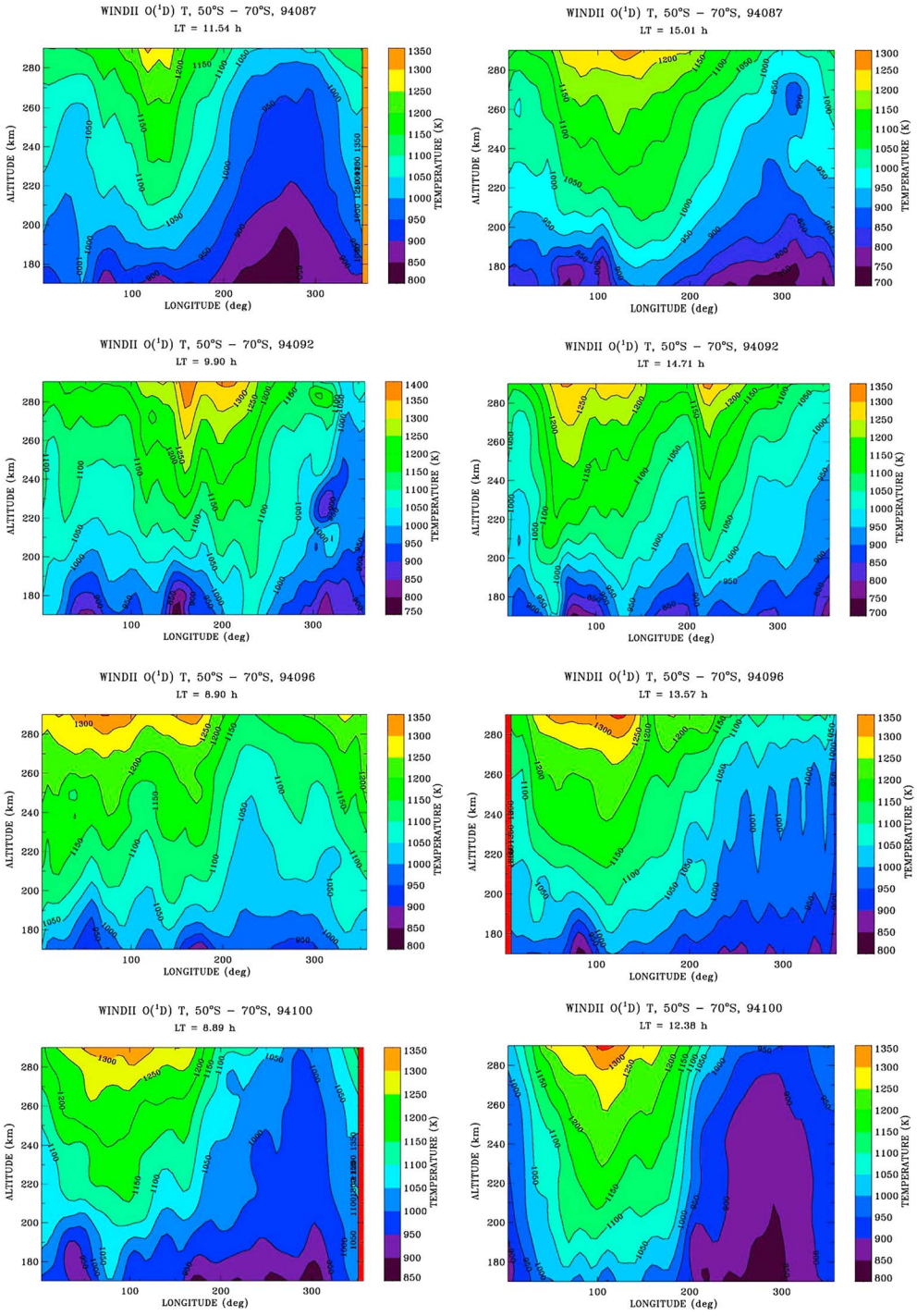

Figure 4. WINDII O(^{1}D) Doppler temperatures at 50°S–70°S as a function of longitude and altitude for the period of 28 March to 10 April 1994 (DoYs 94,087–94,100).

3.3. O(^{1}D) Zonal Winds

Next, the neutral zonal winds derived from the O(^{1}D) observations for the two periods of interest are examined. Figure 6 (March/April 1994) shows the global variations of the zonal wind with height and longitude for the latitude range of 50°S–70°S. Here positive values indicate eastward flow for the zonal wind. In the morning hours (left column) there is a westward peak over 50°E–160°E, with the exception of DoY 94,087, where the wind field is eastward and the wind at ~150°E is decreasing with increasing height. In

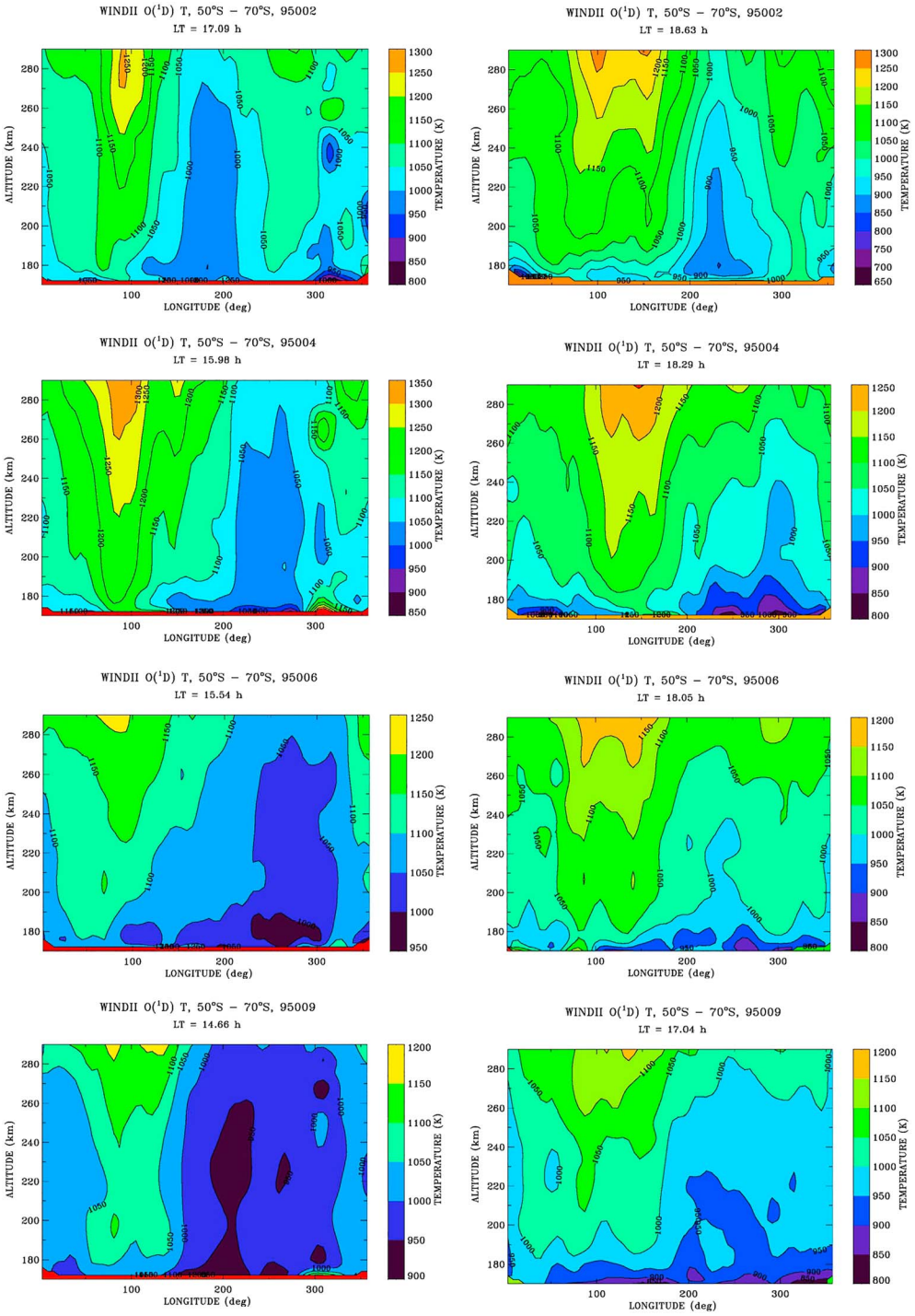

Figure 5. The same as in Figure 4 but for the period of 2–9 January 1995 (DoYs 95,002–95,009).

the afternoon (right column) the zonal wind appears almost entirely westward (negative), reaching a trough at the same region as the peak O(^{1}D) VER. (Note that the color scales are different for each image.)

A similar zonal wind pattern is observed during January 1995 in Figure 7. Although the local time coverage is from 11.1 LT to 14.2 LT, for the descending part of the orbit, and from ~17.5 LT to 19 LT for the ascending, there are striking similarities with the wind observations from March/April 1994; in that, the region of ~50°E–200°E is marked either by weakening of the eastward winds or reversal of direction to westward.

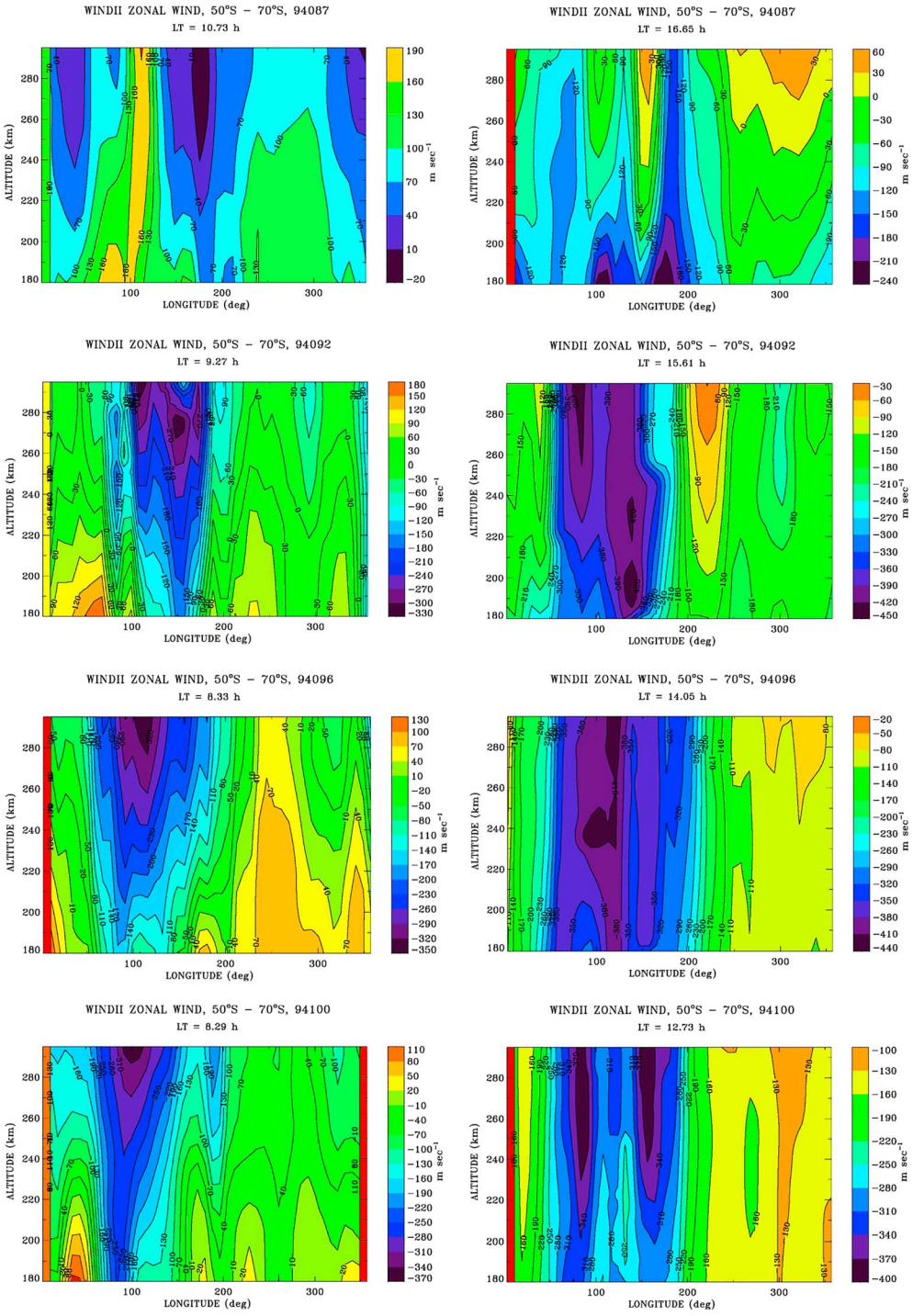

Figure 6. WINDII O(^{1}D) zonal winds at 50°S–70°S as a function of longitude and altitude, for the period of 28 March to 10 April 1994 (DoYs 94,087–94,100). Here the zonal wind velocity is positive for eastward direction and negative for westward direction.

An exception to this pattern is DoY 95,009, which does not show westward winds (Figure 7, bottom left panel), but only weakening of the eastward wind with a minimum at ~100°E most apparent below 250-km height as well as having other features across all longitudes. In the late afternoon/early evening (right column) the zonal wind is entirely westward with a trough in the 50°E–200°E longitude range. In the early afternoon (left column) there are strong zonal eastward winds with a peak velocity of 100–150 m/s

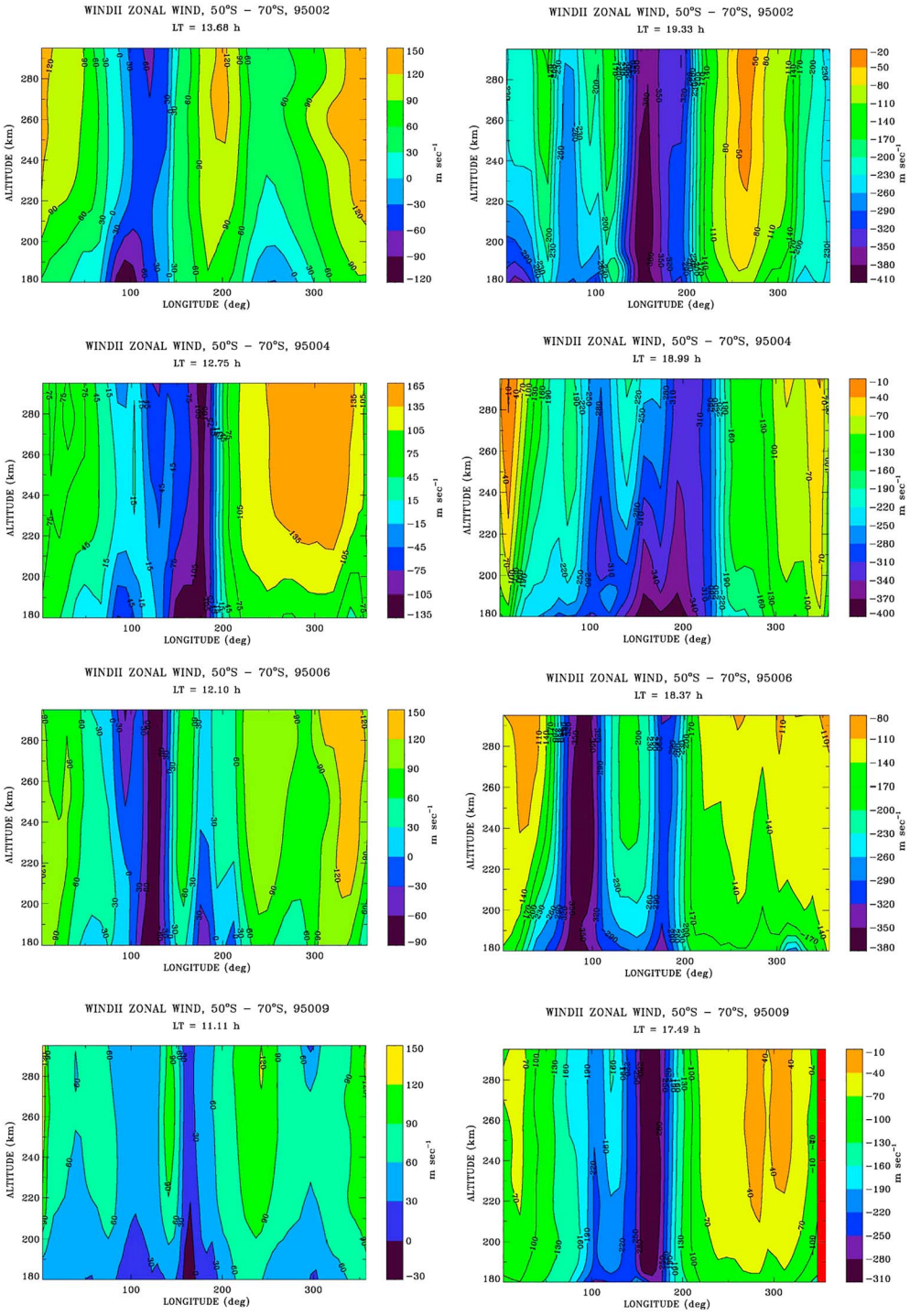

Figure 7. The same as in Figure 6 but for 2–9 January 1995 (DoYs 95,002–95,009).

at 200°E–50°E. The zonal wind in the late afternoon (right column) is entirely westward with a series of individual profiles reaching velocities of up to −450 m/s, all observed at 100°E–200°E.

Maps of the zonal wind for summer solstice at 250 km between 50°S and 70°S, shown in Figure 8, indicate that the observed reversals and troughs in the zonal wind originate around noon at latitudes poleward of 67°S and in the longitude range of 100°E–200°E, expanding equatorward with increasing local time. The westward wind velocity around noon gradually decreases in magnitude from day to day while

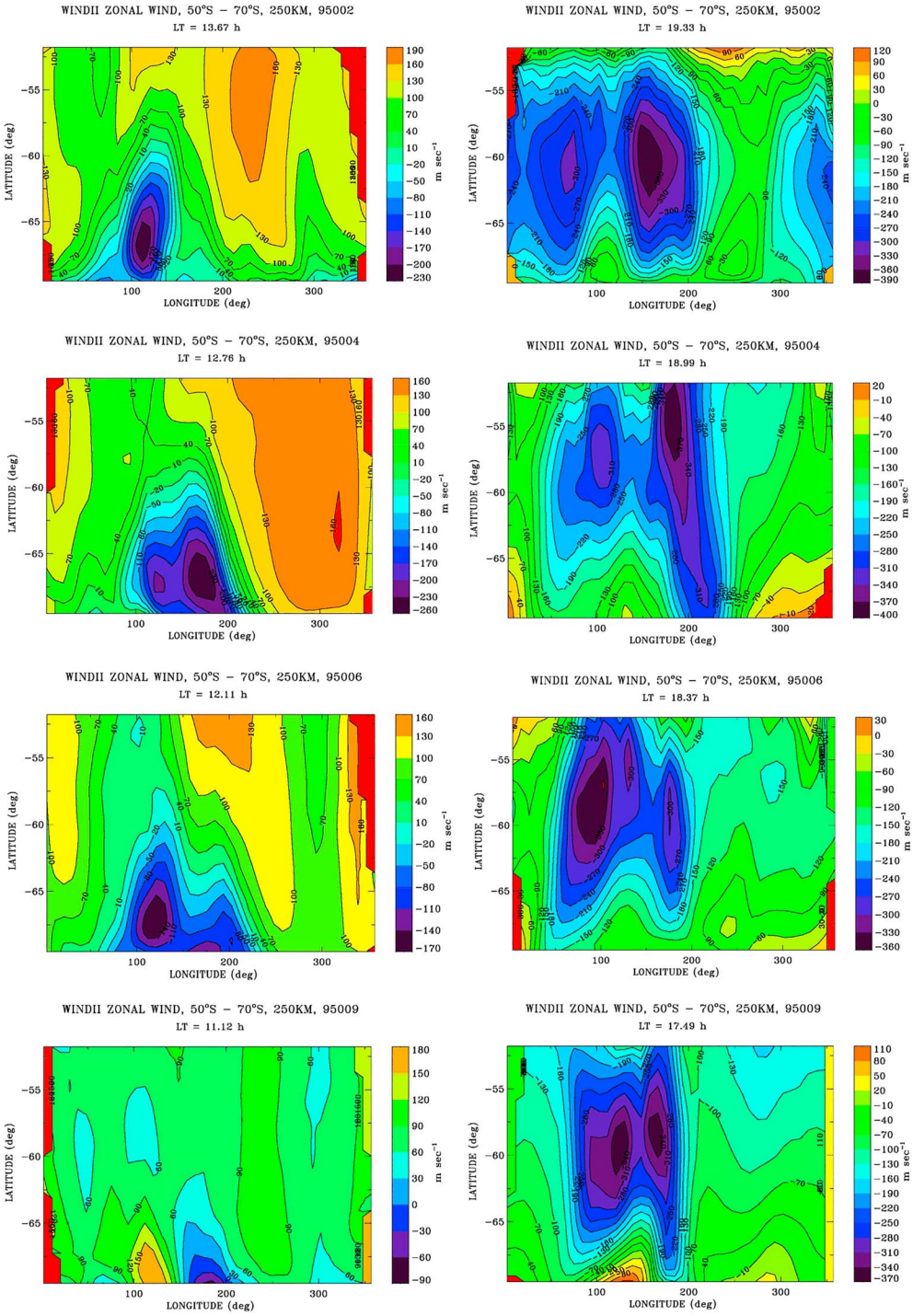

Figure 8. Maps of the zonal wind at 50°S–70°S and 250-km height, for the period of 2–9 January 1995 (DoYs 95,002–95,009).

maintaining its position poleward of ~63°S. A similar day-to-day pattern is observed in the evening sector, when the peak westward wind reached a velocity of −350 to −400 m/s. The structure remained at this location unperturbed over the entire period of 2–9 January 1995.

3.4. O(^{1}D) Meridional Winds

The meridional wind for the period of 28 March to 10 April 1994 at 50°S–70°S is shown in Figure 9, with local time between 8.4 LT and 11 LT for the descending part of the orbit (left column) and from 12.7 LT to 15.3 LT

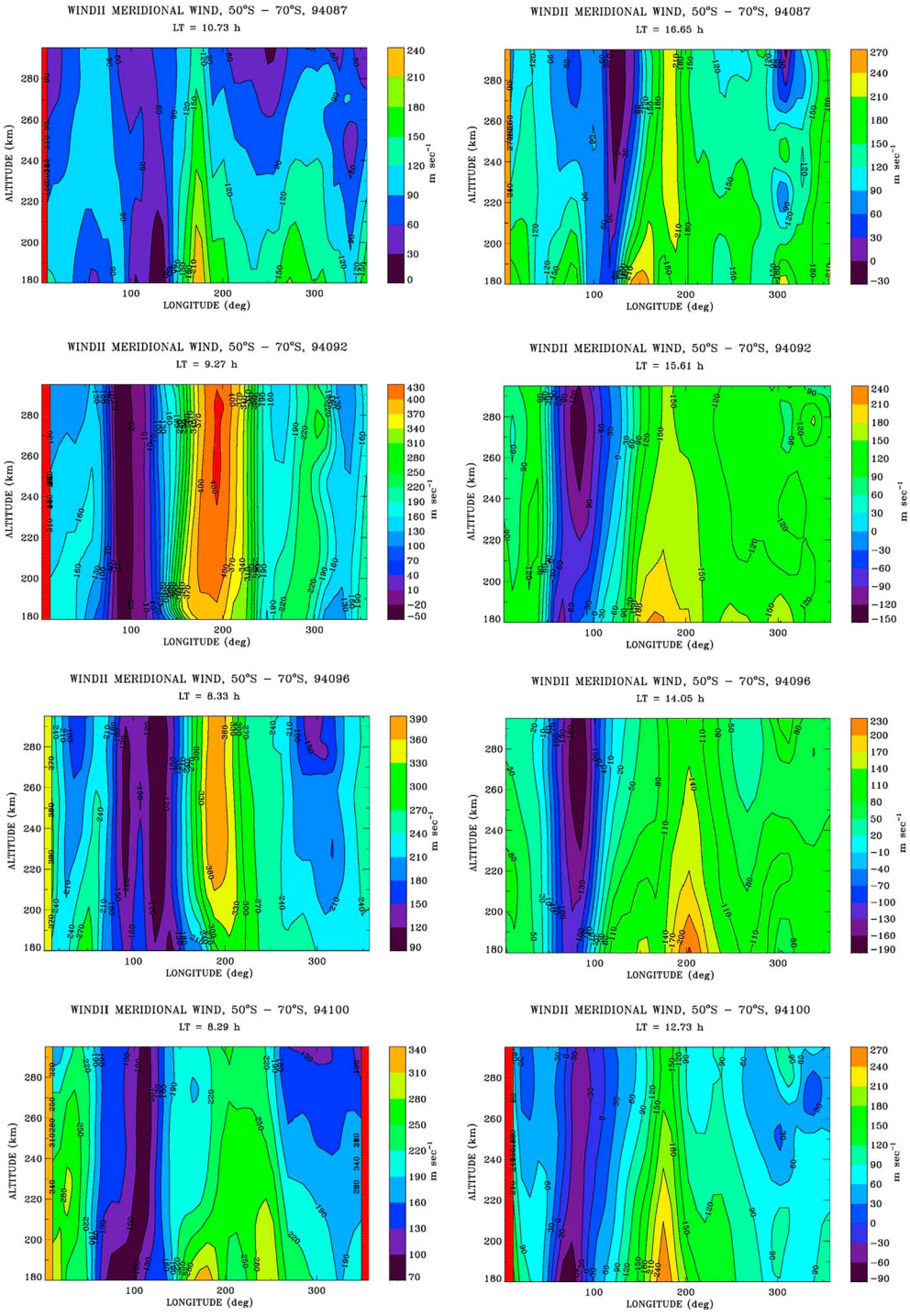

Figure 9. WINDII meridional winds at 50°S–70°S as a function of longitude and altitude for 28 March to 10 April 1994 (DoYs 94,087–94,100). Here the meridional wind speed is positive for north/equatorward direction and negative for south/poleward direction.

for the ascending part (right column). A persistent signature in these plots is the peak of meridional wind northward (positive) speed at ~150°E–250°E, which is accompanied by a trough of decreased northward wind in the morning period or southward wind at 50°E–150°E during the afternoon.

The meridional winds at 50°S–70°S for the period of 2–9 January 1995 presented in Figure 10 show a similar pattern to that observed during fall equinox 1994 (Figure 9). The observations cover a local time period from

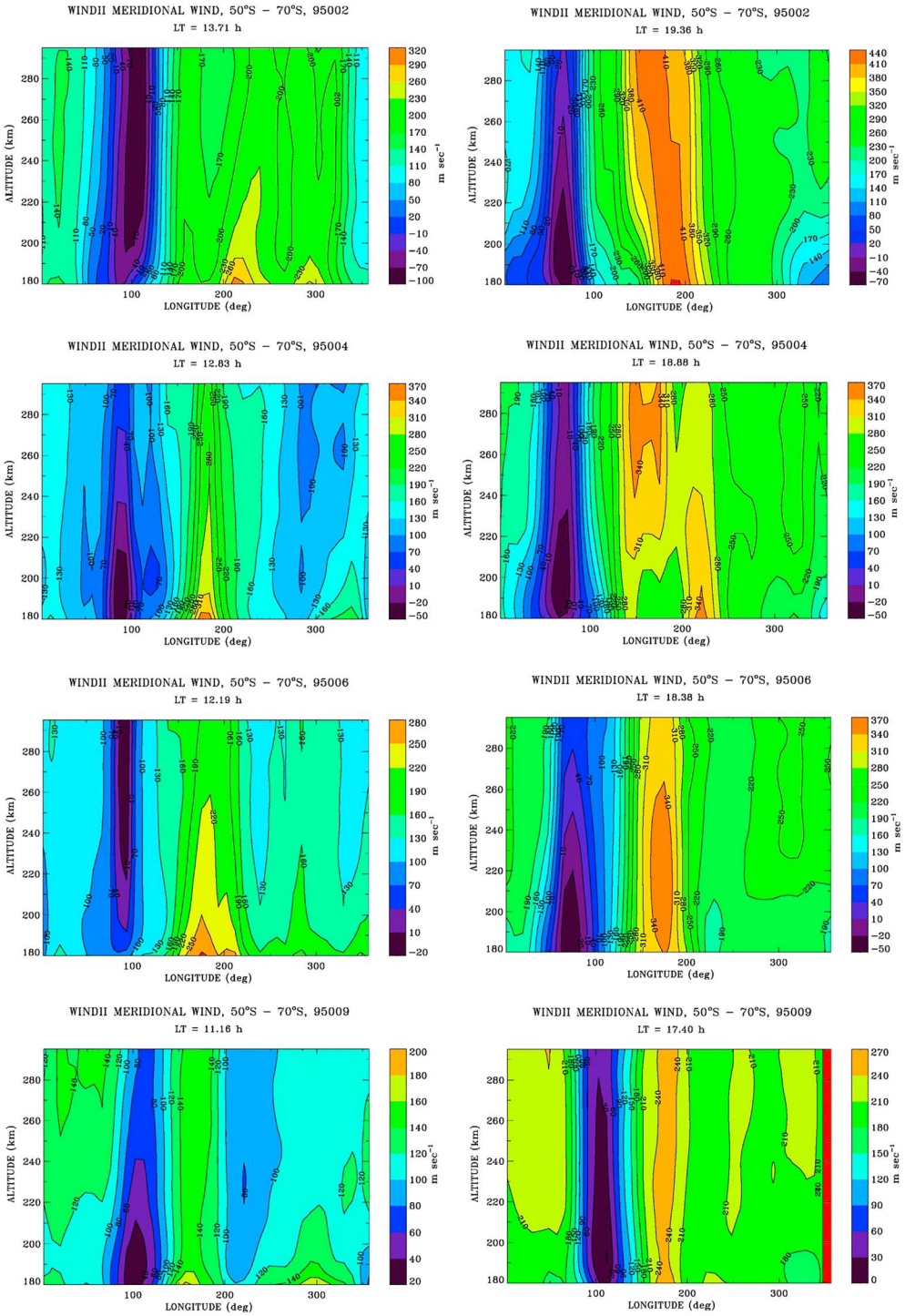

Figure 10. The same as in Figure 9 but for 2–9 January 1995 (DoYs 95,002–95,009).

11.2 LT to 13.7 LT (descending, left column) and 17.4 LT to 19.4 LT (ascending, right column). The general pattern is similar to that observed during March/April 1994, namely, a peak (enhancement) in the northward wind observed at 150°E–250°E and seen in both ascending and the descending observations. The magnitude of this enhancement varies from day to day, but the wind speed can reach as much as 400 m/s and its peak is persistently within the 150°E–250°E region. Also, similarly to the fall equinox, there is a region of decreased northward or southward meridional wind with a trough centered at ~70°E–100°E.

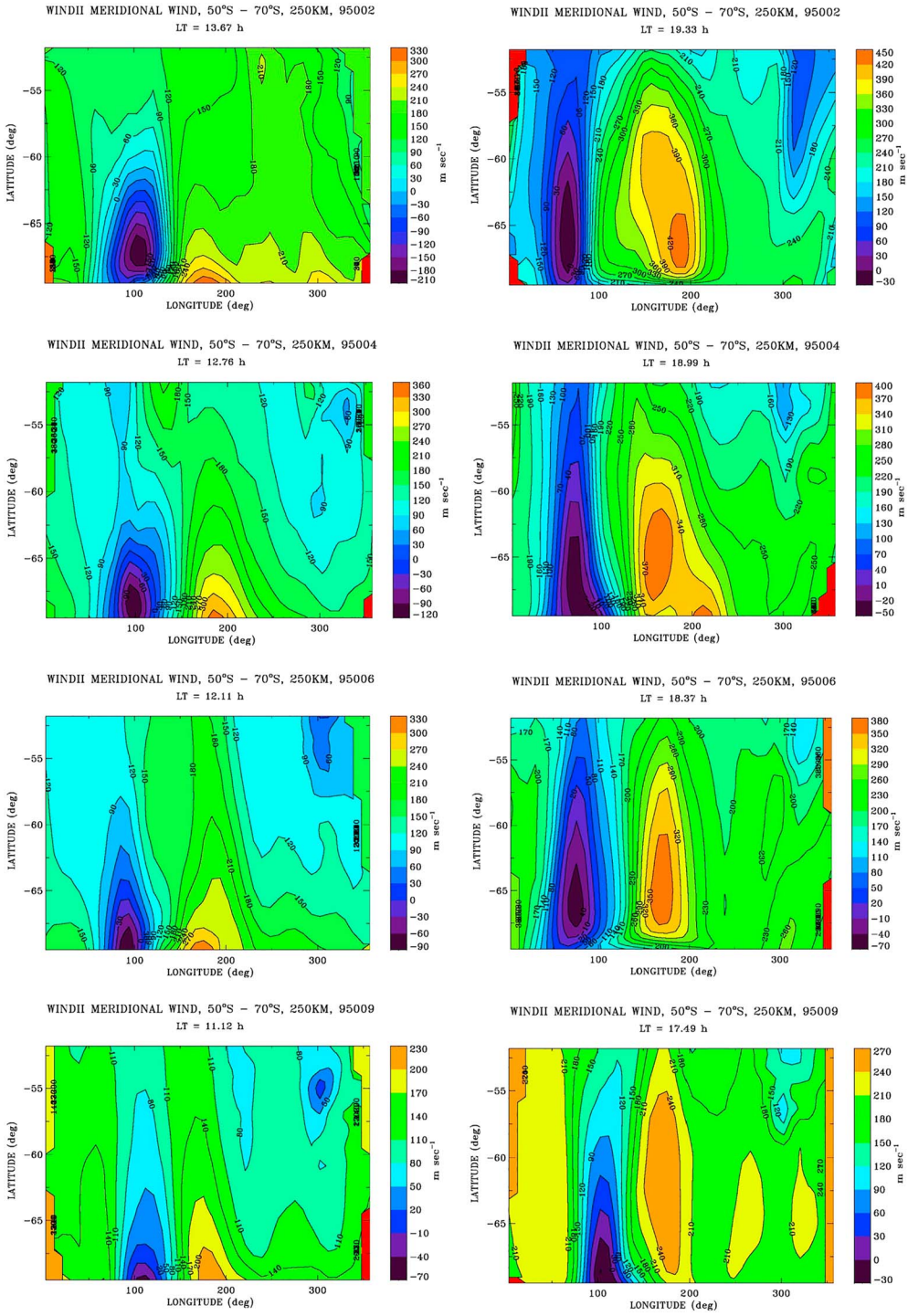

Figure 11. Maps of meridional wind at 50°S–70°S and 250-km height for the period of 2–9 January 1995 (DoYs 95,002–95,009).

In summary, independently of day, local time, and season to the extent that this can be addressed with the available data, the region of 50°E–250°E is characterized by a double signature of a peak meridional wind at ~150°E–250°E and a trough at 50°E–100°E.

Daily maps of the meridional wind field at 50°S–70°S and 250-km height are shown in Figure 11. The same remarkable combination of two narrow adjacent regions of northward and southward winds is evident; the

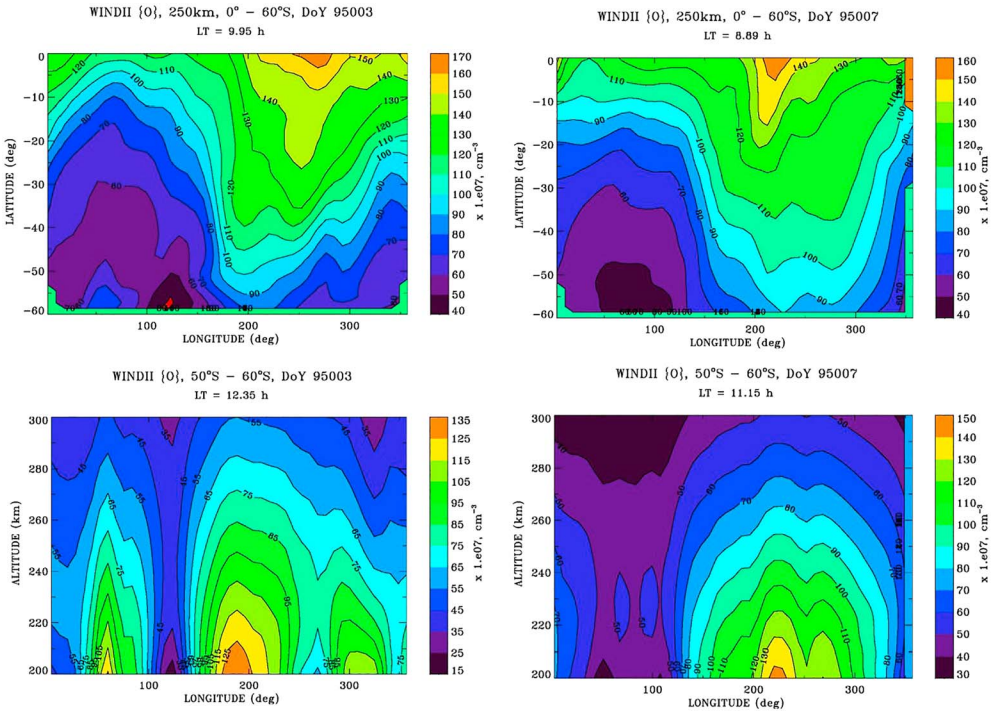

Figure 12. (top row) Maps of the [O] derived from the WINDII O^+ 732–733-nm airglow observations for 3 January 1995 (DoY 95,003) and 7 January 1995 (DoY 95,007) at 250-km height from 0° to 60°S. (bottom row) The derived [O] as a function of longitude and altitude at 50°S–60°S.

southward winds are observed at latitudes higher than 65°S. Around noon (11.1 LT–13.7 LT) the peak/trough signatures observed at ~66°S–70°S extend equatorward to about 60°S, while in the early evening period (17.4 LT–19.4 LT) they can be seen stretching further, to ~50°S, with the trough equatorward of 60°S indicating a reduced northward wind.

3.5. WINDII [O] Observations

As was mentioned earlier, one of the main production mechanisms for daytime $O(^1D)$ VER is the photoionization of atomic oxygen. To understand better the source of the perturbations observed in the $O(^1D)$ VER the atomic oxygen densities derived from the WINDII O^+ 732–733-nm VERs are also examined. Data from 3 and 7 January 1995 (DoY 95,003 and 95,007) are within the time period of the solsticial WINDII observations considered in this study, flanked by the $O(^1D)$ observations on 2 and 4 January 1995 and 6 January 1995 (DoYs 95,002, 95,004, and 95,006, respectively).

Figure 12, top panel, shows maps of all [O] observations at 250 km on 3 January 1995 (DoY 95,003) and 7 January 1995 (DoY 95,007) from 0° to 59°S latitude, thus including the region of low and mid-southern latitudes, examined in M. Shepherd (2016, 2018). The "cutoff" latitude of 59° results from the original model simulations by G. Shepherd et al. (2016) and is associated with the model solar flux that is difficult to calculate for large solar zenith angles. South of the equator the [O] field appears as a wave 1 with a depletion of [O] south of ~20°S and west of ~150°E–200°E. The depletion of O near 100°E longitude and 40°S latitude, originally reported by G. Shepherd et al. (2016), clearly extends closer to the equator than do the perturbations in $O(^1D)$ VER and the zonal and meridional winds. Figure 12, bottom panel, shows the [O] global variability with height over the altitude range of 200–300 km and at 50°S–60°S.

3.6. TOPEX TEC Observations

Global maps of TOPEX TEC at the latitude band of 50°S–67°S for the period of 28 March to 10 April 1994 (DoYs 94,087–94,100), fall equinox, are shown in Figure 13. As in the WINDII case, the data are divided into the descending and ascending parts of the TOPEX orbit with local time from 7.2 LT to 9.7 LT (descending, left column) and 11.8 LT to 14.5 LT (ascending, right column).

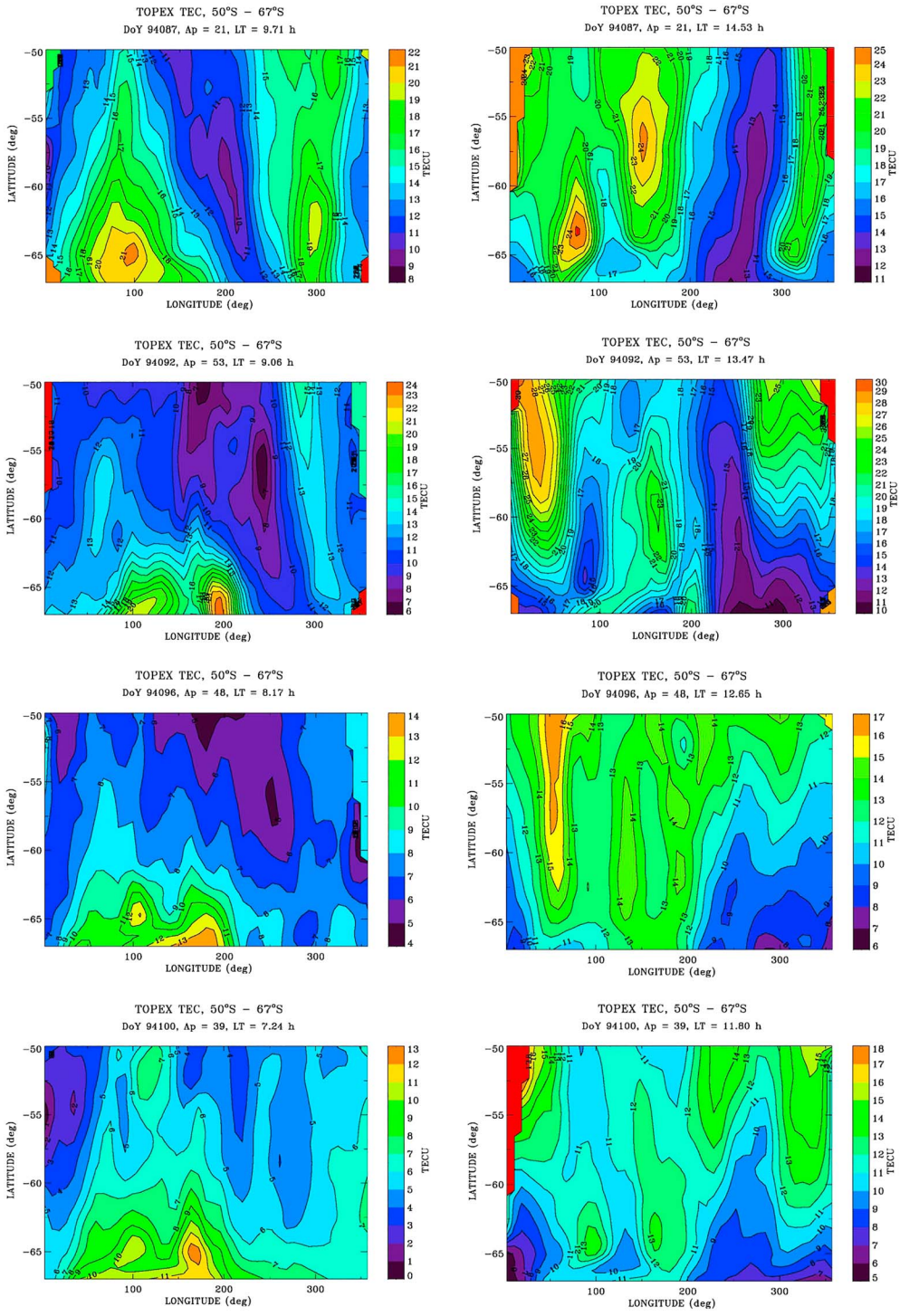

Figure 13. Maps of TEC observations by the TOPEX satellite over the latitude range 50°S–67°S for the period of 28 March to 10 April 1994 (DoYs 94,087–94,100), the days of the WINDII observations, presented in this study.

In the morning hours, during the descent (Figure 13, left column), the TEC shows an enhancement at 50°E–200°E with a peak at ~65°S–67°S. Another weak enhancement is seen at ~300°E and cannot even be distinguished in the later part of the period (e.g., DoYs 94,096–94100). For DoY 94,087 with $Ap = 21$ the enhancement extends to ~50°S (for morning, left column) but for subsequent days of large Ap (39–53) the enhancement is confined to higher latitudes. This is not so for the noon observations (right column).

During the noon/early afternoon period (Figure 13, right column), the TEC enhancement broadens in longitude from 50°E to 200°E and extends throughout the entire latitude band showing a distinct double signature with peaks at ~50°E and 150°E, which varies in strength but remains more or less "locked" over this longitude region. The enhancement at ~300°E is also present.

The local time coverage of the TEC observations during the 28 March to 10 April 1994 period, shown in Figure 13, is very close to the local time of the WINDII O(^{1}D) VER observations, shown in Figure 1. There appears to be a good longitudinal and temporal correspondence between the peak TEC and the peaks of the O(^{1}D) VERs. There is also a good correspondence between the maps of O(^{1}D) VER at 250-km height, shown in Figure 3 and the TEC observations for the same period. In conclusion, one persistent pattern exists, namely, the increase of TEC at 0°E–200°E during southern fall equinox as shown in Figure 13.

Maps of the TEC observed by TOPEX for the period of 2–9 January 1995 are shown in Figure 14, with local time from 23.6 LT to 0.5 LT, for the descending part of the orbit (left column) and from ~4.3 LT to 5.1 LT for the ascending portion (right column). Because of the different orbit precessions from day to day between WINDII and TOPEX it is difficult to find persistently good local time correspondence between the two experiments, as illustrated by Figure 14. During descent the TEC observations are around local midnight, while the ascending data are for early morning preceding the WINDII observations by 11–12 hr (e.g., DoY 95,002). The TEC global distribution around local midnight (left column) shows an enhancement at the longitude region of ~200°E–360°E that extends over the entire latitude range of 50°S–67°S. The region of ~0°E to 200°E shows a decreased/depleted TEC also throughout the examined latitude band. During the ascending part of the orbit, in the early morning hours (right column) the TEC peak is still observed around 300°E, and its longitude extent reached ~50°E, while the trough that was seen around 0°–100°E at midnight now appears moved eastward to 50°E–200°E.

In an attempt to further examine the daytime TEC variability in summer and its relationship to the observed WINDII parameters TEC observations from three consecutive summer seasons (January/February) in 1994, 1995 and 1996 were also considered. From these the observations from February 1996 (2–12 February 1996) were within the range of local times observed by WINDII during 2–9 January 1995. Figure 15 shows TEC maps of some of these observations for 13.7 LT to 15.6 LT (left column) and for 18.4 LT to 20.4 LT (right column). Here the TOPEX and WINDII observations are correlative in local time (daytime), season (summer), and geomagnetic activity (low, $Ap = 6$–14), although they are not exactly on the same date. What Figure 15 shows is that the longitude position of the TEC enhancement is dependent on local time and for daytime it is at 50°E–250°E, the region where O(^{1}D) VER and Doppler temperature also peak. Through the local night, the TEC peaks at about 200°E–300°E with a secondary enhancement still present at 100°E–150°E, as illustrated by Figures 14 and 15 (right column). Figure 15 also shows that the extent of TEC depletion at 0°–100°E is also dependent on local time in terms of its latitudinal extent.

What is significant about Figure 14 is that the longitude range of TEC depletion overlaps with the range of depleted [O] as depicted in Figure 12. That is, the electron density, Ne as indicated by the TEC (e.g., DoYs 95,002 and 95,004) and the [O] (e.g., DoY 95,003) as observed by WINDII, corresponds to one another in their longitude ranges.

It is well known (e.g., Rishbeth, 1998) that the production and loss of electron density Ne and TEC depend on the neutral composition through the [O]/[N_2] density ratio, as the Ne production depends mainly on [O], while the Ne losses depend mainly on N_2 with a small contribution from O_2. The TOPEX TECs at 50°S–67°S during January 1995 as shown in Figure 14 (around local midnight, left column) and during February 1996 in Figure 15 (evening, right column) appear to have a similar pattern with the atomic oxygen [O] at 50°S–60°S (noon; Figure 12), thus suggesting a close association of Ne with [O] in spite of the difference in local times.

The geomagnetic activity characterized by the *Ap* index for each of the days during fall equinox considered shows moderate geomagnetic activity during the 28 March to 10 April 1994 period with *Ap* values of 21–53, for the days presented. On 3 April (DoY 94,093), the *Ap* reached 93 ($Kp = 5-$). On 2 April 1994 (DoY 94,092), the observed TEC was considerably higher (up to 30 TECU), with a peak at ~50°E, which decreased in strength, but remained present over the course of the following days. The geomagnetic activity during 2–6 January 1995 is low with *Ap* on the order of 16–18, dropping to 7 by 9 January 1995.

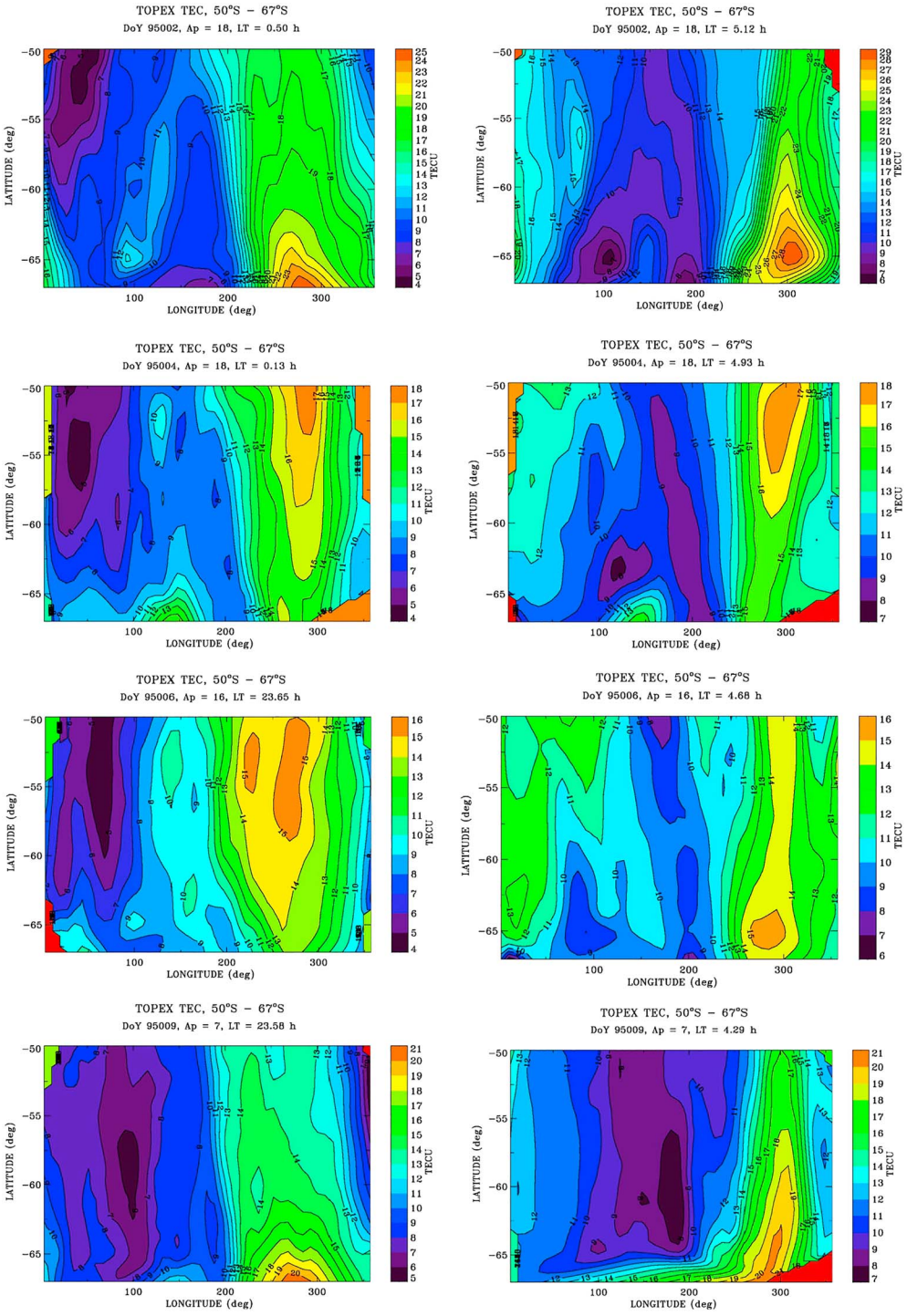

Figure 14. The same as in Figure 13 but for 2–9 January 1995 (DoYs 95,002–95,009).

The overlapping of the region of equinox peak TEC with the peak O(^{1}D) for the same season is consistent with photoelectron impact on O as a production mechanism. During the transition from summer to fall equinox in the thermosphere at the latitudes considered here the mean molecular mass decreases, while the atomic oxygen increases. This is the result of the downwelling and increased [O]/[N_2] ratio, caused by O convection from the summer to winter hemisphere, particularly over the Australasian sector (~100°E–150°E) as described by Rishbeth (1998). Although the solar zenith angle increases, its effect is not significant as

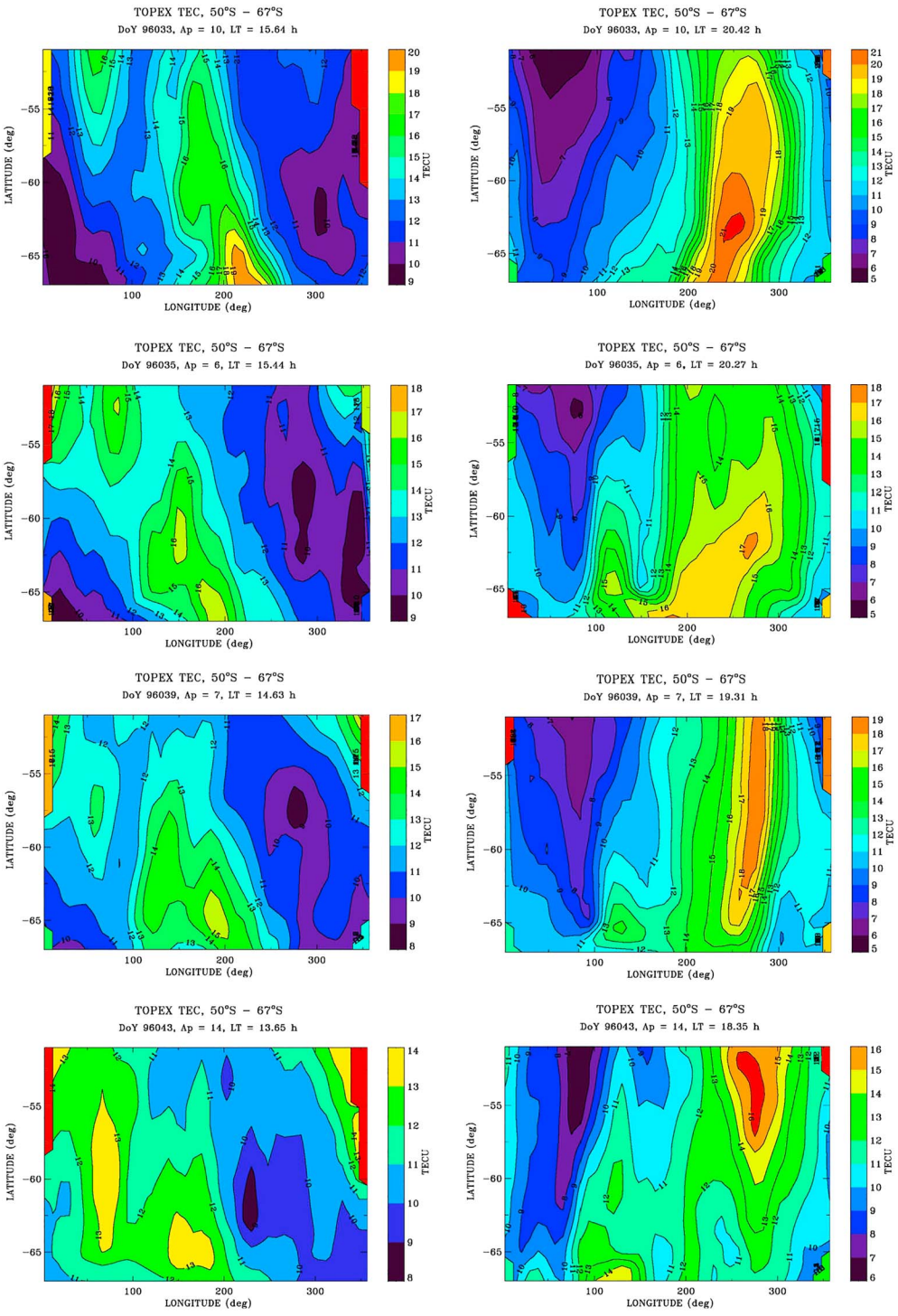

Figure 15. Selected maps of TEC observations from 2–12 February 1996 (DoYs 96,033–96,043) correlative to the WINDII observations in local time (left column), season (summer solstice), and geomagnetic activity (low, Ap = 6–14).

indicated by the persistent longitudinal pattern observed independently of local time and day. It is also evident that during fall equinox at least for the noon/early afternoon period (Figure 13, right column) there is TEC depletion that extends further poleward than 67°S across a range of longitudes (200°E–50°E), somewhat similar to the reduced O(^{1}D) VER at these latitudes as shown in Figure 3 for equinox. Seasonal variability may also be involved in some way, perhaps through the general circulation, but it is not

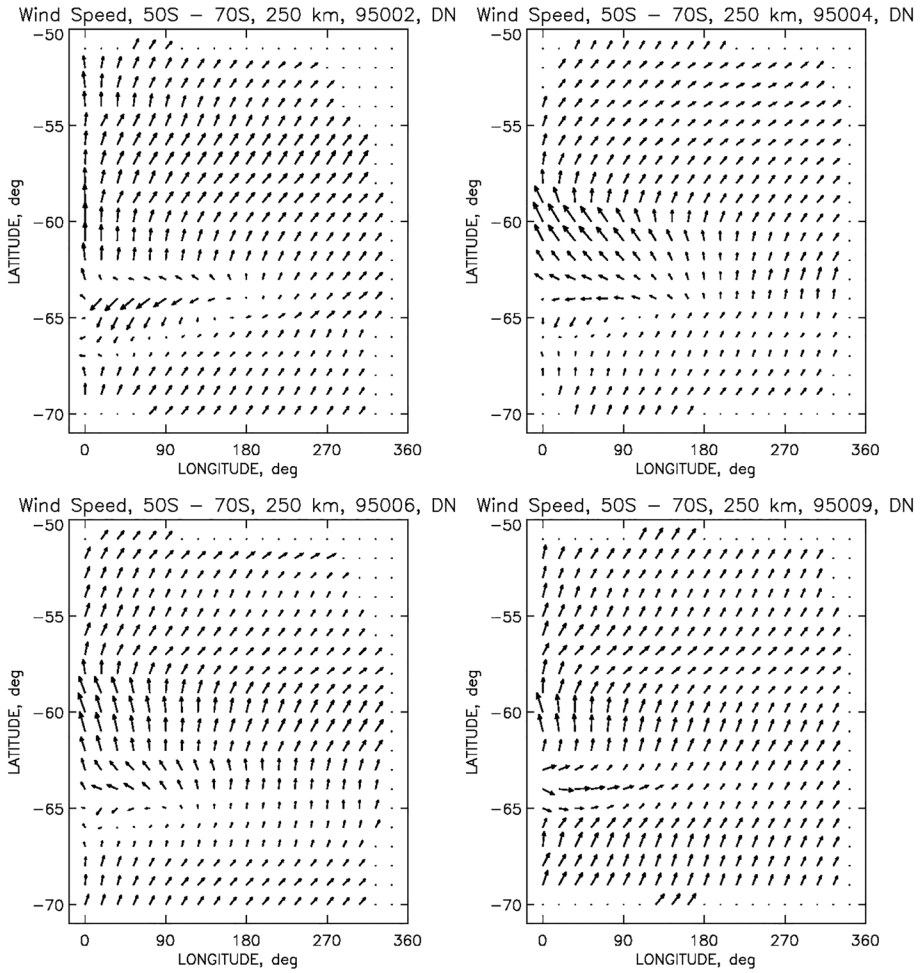

Figure 16. Maps of wind velocity vector at 250-km height and 50°S–70°S, for 2–9 January 1995 (DoYs 95,002–95,009) at 11 LT–14 LT (descending data set). The size of the velocity vectors is normalized to the largest value for each of the plots.

evident that this would involve a longitudinal variation. The pattern is reversed during the local night indicating local time dependence (Figure 14, left column and Figure 15, right column).

4. Wind Velocity Vectors

The WINDII zonal and meridional wind observations allow the estimation of the neutral wind vector velocity within the latitude band of 50°S–70°S, for an altitude of 250 km. The daily maps of the wind velocity vector in geographic coordinates for the descending part of the WINDII orbit, 11 LT–14 LT, during the 2–9 January 1995 period are shown in Figure 16. The wind velocity vector is directed mostly north-eastward except for the region at 0°–180°E and ~60°S (58°S–63°S) where the wind velocity vector is northward to north-westward. Around 63°S–66°S the wind sharply decreases and reverses direction to south-westward, as seen on DoYs 95,002–95,006. It appears as if there is a "wall" in the neutral wind at ~63°S–66°S, but it is more a longitudinal structure, where the wind velocity vector diverts both poleward and equatorward, with enhanced wind velocity vector appearing equatorward of the wall. The region of minimum wind velocity, 66°S and 130°E, the region of wind reversal, is also the location of the southern magnetic pole (64.8°S, 138.7°E, in 1995).

5. Discussion

One of the first reports on the longitudinal variability of the neutral atmosphere at Southern middle and high latitudes was by Laux and von Zahn (1979) employing monopole mass spectrometer data from the Esro 4

satellite. They reported drastic changes in the $[O]/[N_2]$ ratio observed between 50°S–80°S and 110°E to 180°E geographic, over the African-Australian sector, within the vicinity of the geomagnetic pole, but shifted by ~10° in latitude toward the equator. As is presented in the current study the N_2 and O extreme variations occurred at the same longitude range independently of local time, remaining fixed to a limited longitude band. The persistence of the observed phenomenon and the lack of strong correlation with geomagnetic activity led Laux and von Zahn (1979) to the conclusion that this is a regular feature associated with thermospheric air motion.

Various studies on the seasonal and longitudinal variability of ionospheric daytime Ne and TEC (e.g., Liu et al., 2009; Mendillo et al., 2005; Millward et al., 1996 and references therein) have shown that these parameters exhibit variability, related to changes in the thermospheric composition, in particular of the $[O]/[N_2]$ ratio. Millward et al. (1996) proposed a theory to explain the observed seasonal and semiannual variations of electron density only through the longitudinal dependence of the interface between the solar-driven low/middle-latitude neutral atmosphere circulation and the geomagnetically driven high-latitude circulation, where the latitude of the interface depends on longitude. In the vicinity of the magnetic pole the magnetically driven circulation extends to relatively low geographic latitudes, and on the dayside its interaction with the neutral atmosphere circulation occurs at a geographic latitude of about ~50°–65°. According to Rishbeth (1998) solar and geomagnetic control on the quiet time thermosphere at midlatitude is characterized by general upwelling in summer (leading to decreased $[O]/[N_2]$) and downwelling in winter (and increased $[O]/[N_2]$). During the transition from summer to equinox in the vicinity of the magnetic pole, the mean molecular mass of the thermosphere at F_2 heights (approximately the height of the peak $O(^1D)$ VER) decreases, from more molecular (smaller $[O]/[N_2]$ ratios) in summer to less molecular (higher $[O]/[N_2]$ ratios) toward equinox. In the vicinity of the magnetic pole changes in the peak electron density depend more on changes in the neutral composition ($[O]/[N_2]$ ratio) than on the solar zenith angle and thus Ne experiences predominantly seasonal variations. Away from the magnetic pole, and the auroral oval, the downwelling and compositional effects are small compared to the effect of the solar zenith angle, which leads to predominantly semiannual (equinox–solstice) variations.

The TEC observations during fall equinox (DoYs 94,087–94,100; Figure 13) showed an enhancement over the region near the magnetic pole, at 50°E–200°E. There is a striking correspondence between the peak longitude of the TEC and the $O(^1D)$ VER, expressed both as a composite of all vertical $O(^1D)$ VER profiles between 50°S and 70°S (Figure 1) and the $O(^1D)$ VER maps at 250 km (Figure 3). In the morning hours (before noon) a peak of $O(^1D)$ VER is observed at the same longitude as the peak in the TEC, at ~150°E–200°E, except on DoY 94,087, where the WINDII observations at 12.1 LT differ by ~3 hr from those of the TEC at 9.7 LT. (We remind the reader that the WINDII local time at a given latitude changes by 20 min from day to day, while the TOPEX day-to-day local time changes by 8 min.) There is a very good correspondence between the two parameters in the noon/afternoon hours as well, where the peak $O(^1D)$ VER is observed at practically the same longitude as that in TEC. Although the TOPEX TEC observations during the summer solstice period of 2–9 January 1995 (DoYs 95,002–95,009) cover the local midnight-dawn period additional observations from 2–12 February 1996 (DoYs 96,032–96,044) for the same local times and geomagnetic activity have shown that the TEC enhancement at 100°E–200°E is a persistent daytime signature during summer and correlates well with the observed peak/troughs of the WINDII parameters.

As was shown there is a longitudinal wind wall at about 63°S–66°S seen in the mapped wind velocity vector, where the neutral wind velocity decreases and/or reverses direction affecting the variability of the $O(^1D)$ VER, TEC, and [O] observed. An interesting feature in the observed variability was the fact that the $O(^1D)$ VER peak in the vicinity of the magnetic pole was a persistent longitudinal feature independent of season and daytime local time. This is even more striking considering the fact that the observations are for different although consecutive days and different local times determined by the precession of the WINDII/UARS orbit. The same pattern is seen in both the zonal and meridional winds.

The correlative in local time observations of TEC, during the fall equinox period of interest, have also shown a persistent enhancement within the longitudinal region of the $O(^1D)$ VER peak. The latitudinal extent and magnitude of the TEC peak varies with local time and geomagnetic activity, but remains almost constant in longitude. The longitudinal variability observed in all parameters considered, and particularly the features observed in the vicinity of the southern magnetic pole, suggested that there might be a common source

related to the so-called midlatitude main ionospheric trough. The main ionospheric trough has usually been discussed in terms of a sharp decrease in nighttime electron density in both hemispheres with steep poleward and equatorward boundaries. By definition (e.g., Rodger et al., 1992) the midlatitude trough is "the region of low plasma concentration at *F* region altitudes that occurs near the equatorward side of the low-latitude edge of the energetic electron precipitation boundary of the auroral oval." Mallis and Essex (1993) have shown that in the Southern Hemisphere the midlatitude main ionospheric trough is often observed during daytime, with particularly strong manifestations in summer and autumnal equinox, the seasons considered in the current study. The authors employed a ground-based differential–phase technique to receive from McQuarrie Island radio transmissions of the NNSS (Navy Navigation Satellite System) polar orbiting satellite to make measurements of the latitudinal variations of ionospheric TEC in the Southern Hemisphere. They found a relatively high incidence of daytime troughs while the incidence of a nighttime trough was relatively low. The Mallis and Essex (1993) observations showed the Southern Hemisphere trough to be an ionospheric feature that develops in early to midafternoon in all seasons that was interpreted as resulting from a two-cell convection pattern of the high-latitude *F* region magnetospheric electric field. The WINDII vector winds for January 1995 appear to have characteristics similar to those of the daytime trough as described by Mallis and Essex (1993), but the available data are insufficient to draw a more definitive conclusion.

Downward motion of the atmosphere brings down air of higher temperature and reduced atomic oxygen as observed. What is initially puzzling in the presented WINDII results is that where the $O(^1D)$ VER increases, the [O] decreases. However, at high latitudes the solar zenith angles are large even in summer time, so that the normally dominant $O(^1D)$ reaction, photoelectron impact excitation of [O], $O + e_{ph} \rightarrow O(^1D) + e_{ph}$ is greatly reduced, as well as the photodissociation of O_2, because the solar flux is small. The other reactions that produce $O(^1D)$ involve O_2 (or O_2^+) but not O. The [O] can be reduced without having much effect on the $O(^1D)$ emission rate. The "other" reactions are dissociative recombination of O_2^+ by thermal electrons, $O_2^+ + e_{th} \rightarrow O(^1S) + O(^1D)$ and $O_2^+ + e_{th} \rightarrow O(^1D) + O(^1D)$. For these the $O(^1D)$ increases with the electron density, so the result is compatible with the TEC data even with reduced O. The TEC is a vertically integrated quantity, so vertical motions would seem to have little influence. Here horizontal motions may be more important, and may be the origin of the TEC variations observed.

6. Summary and Conclusions

The study led to the following conclusions, applicable to the Southern Hemisphere:

1. The $O(^1D)$ VER for Southern Hemisphere fall equinox (March/April 1994) and summer solstice (January 1995) at 50°S–70°S revealed a peak in the emission rate over the longitude range of 50°E–200°E for both seasons and local times varying from 9 LT to 19 LT. The Doppler temperatures obtained from the $O(^1D)$ emission also exhibited a maximum at the same location, for both seasons and the same range of local times.
2. The zonal winds were predominantly westward at the same location, reaching wind speeds of as much as 450 m/s. The wind field has a wave-1 like structure with an eastward peak at 200°E–360°E and a westward trough at 50°E–200°E.
3. Meridional winds show a "peak and trough" structure over the same region, 50°E–200°E, with a distinct eastern boundary at ~150°E showing a peak of equatorward (positive, northward) meridional wind centered at ~200°E, and a western boundary at ~50°E with a trough in the meridional wind (weak northward or southward), centered at 70°E–100°E.
4. The atomic oxygen is depleted during summer solstice at the region of the $O(^1D)$ VER enhancement in the presence of westward zonal wind and a weak or reversed meridional wind.
5. Contemporaneous TEC observations showed a peak that coincided with the $O(^1D)$ VER enhancement during the equinox period. It showed a minimum TEC coincident with the maximum $O(^1D)$ emission during the summer solstice but this may be a result of the nighttime local time of the TEC observations.
6. The vector wind pattern appears to have characteristics similar to some of the daytime main ionospheric troughs as described by Mallis and Essex (1993), but more information is needed for a positive identification of the source of the longitudinal variability as described in this study. The region of minimum wind is near the magnetic pole.

7. The neutral winds appear to be the driver of the O(^{1}D) enhanced emission, the Doppler temperature increase, and the enhanced TEC through downward motion of air from above. This downward air motion is characterized by higher temperature and higher electron density that produces the enhanced O(^{1}D) emission, all during the equinox period.

Acknowledgments
The authors would like to acknowledge the members of the WINDII team. The WINDII project was sponsored by the Canadian Space Agency and the Centre National d'Etudes Spatiales (CNES) with the support of NASA. The WINDII data are available on the Canada Open Data Portal (https://open.canada.ca/data/en/dataset?keywords=WINDII). The raw TOPEX/POSEIDON data used in the study are available via (https://podaac.jpl.nasa.gov/TOPEX-POSEIDON). The processed TOPEX TEC data employed in the study can be obtained on request from Mihail Codrescu (mihail.codrescu@noaa.gov).

References

Codrescu, M. V., Beierle, K. L., Fuller-Rowell, T. J., Palo, S. E., & Zhang, X. (2001). More total electron content climatology from TOPEX/Poseidon measurements. *Radio Science*, *36*(2), 325–333. https://doi.org/10.1029/1999RS002407

Codrescu, M. V., Palo, S. E., Zhang, X., Fuller-Rowell, T. J., & Poppe, C. (1999). TEC climatology derived from TOPEX/POSEIDON measurements. *Journal of Atmospheric and Solar - Terrestrial Physics*, *61*(3-4), 281–298. https://doi.org/10.1016/S1364-6826(98)00132-1

Dhadly, M. S., Emmert, J. T., Drob, P. D., Conde, M. G., Doornbos, E., Shepherd, G. G., et al. (2017). Seasonal dependence of northern high-latitude upper thermospheric winds: A quiet time climatological study based on ground-based and space-based measurements. *Journal of Geophysical Research: Space Physics*, *122*, 2619–2644. https://doi.org/10.1002/2016JA023688

Dhadly, M. S., Emmert, J. T., Drob, P. D., Conde, M. G., Doornbos, E., Shepherd, G. G., et al. (2018). Seasonal dependence of geomagnetic active-time northern high-latitude upper thermospheric winds. *Journal of Geophysical Research: Space Physics*, *123*(1), 739–754. https://doi.org/10.1002/2017JA024715

Fu, L. L., Christensen, E. J., Yamatone, C. A. Jr., Lefebvre, M., Menard, Y., Dorrer, M., & Escudier, P. (1994). TOPEX/POSEIDON mission overview. *Journal of Geophysical Research*, *99*(C12), 24,369–24,381. https://doi.org/10.1029/94JC01761

Gault, W. A., Thuillier, G., Shepherd, G. G., Zhang, S. P., Wiens, R. H., Ward, W. E., et al. (1996). Validation of O(^{1}S) wind measurements by WINDII the wind imaging interferometer on UARS. *Journal of Geophysical Research*, *101*(D6), 10,405–10,430. https://doi.org/10.1029/95JD03352

Lathuillère, C., Gault, W., Lamballais, B., Rochon, Y. J., & Solheim, B. (2002). Doppler temperatures from O^{1}D airglow in the daylight thermosphere as observed by the WINDII interferometer on board the UARS satellite. *Annales Geophysicae*, *20*(2), 203–212. https://doi.org/10.5194/angeo-20-203-2002

Laux, U., & von Zahn, U. (1979). Longitudinal variations in thermospheric composition under geomagnetically quiet conditions. *Journal of Geophysical Research*, *84*(A5), 1942–1946. https://doi.org/10.1029/JA084iA05p01942

Liu, L., Zhao, B., Wan, W., Ning, B., Zhang, M.-L., & He, M. (2009). Seasonal variations of the ionospheric electron densities retrieved from Constellation Observing System for Meteorology, Ionosphere, and Climate mission radio occultation measurements. *Journal of Geophysical Research*, *114*(A2), A02302. https://doi.org/10.1029/2008JA013819

Mallis, M., & Essex, E. A. (1993). Diurnal and seasonal variability of the southern-hemisphere main ionospheric trough from differential-phase measurements. *Journal of Atmospheric and Terrestrial Physics*, *55*(7), 1021–1037. https://doi.org/10.1016/0021-9169(93)90095-G

Mendillo, M., Huang, C., Pi, X., Rishbeth, H., & Meier, R. (2005). The global ionospheric asymmetry in total electron content. *Journal of Atmospheric and Solar-Terrestrial Physics*, *67*(15), 1377–1387. https://doi.org/10.1016/j.jastp.2005.06.021

Millward, G. H., Moffett, R. J., Quegan, S., & Fuller-Rowell, T. J. (1996). Ionospheric F_2 layer seasonal and semiannual variations. *Journal of Geophysical Research*, *101*(A3), 5149–5156. https://doi.org/10.1029/95JA03343

Richmond, A. D., Lathuillère, C., & Vennerstroem, S. (2003). Winds in the high-latitude lower thermosphere: Dependence on the interplanetary magnetic field. *Journal of Geophysical Research*, *108*(A2), 1066. https://doi.org/10.1029/2002JA009493

Rishbeth, H. (1998). How the thermospheric circulation affects the ionospheric F_2-layer. *Journal of Atmospheric and Solar-Terrestrial Physics*, *60*, 1385–1402. https://doi.org/10.1016/S1364-6826(98)00062-5

Rodger, A. S., Moffett, R. J., & Quegan, S. (1992). The role of ion drift in the formation of ionization troughs in the mid- and high-latitude ionosphere—A review. *Journal of Atmospheric and Terrestrial Physics*, *54*(1), 1–30. https://doi.org/10.1016/0021-9169(92)90082-V

Shepherd, G. G., & Cho, Y.-M. (2017). Stationary depletions in thermospheric atomic oxygen concentration and mass density observed with WINDII, GUVI, GOCE and simulated by NRLMSISE-00. *Journal of Atmospheric and Solar-Terrestrial Physics*, *164*, 29–38. https://doi.org/10.1016/j.jastp.2017.07.016

Shepherd, G. G., Cho, Y. M., Fomichev, V. I., & Martynenko, O. V. (2016). Thermospheric atomic oxygen concentrations from WINDII O$^+$ (^{2}P-^{2}D) 732 nm emission: Comparisons with the NRLMSISE-00 and C-IAM models and with GUVI observations. *Journal of Atmospheric and Solar-Terrestrial Physics*, *147*, 50–58. https://doi.org/10.1016/jjastp.2016.06.015

Shepherd, G. G., & Shepherd, M. G. (2018). High-latitude observations of a localized wind wall and its coupling to the lower thermosphere. *Geophysical Research Letters*, *45*(10), 4586–4593. https://doi.org/10.1029/2018GL077722

Shepherd, G. G., Thuillier, G., Cho, Y.-M., Duboin, M.-L., Evans, W. F. J., Gault, W. A., et al. (2012). The Wind Imaging Interferometer (WINDII) on the Upper Atmosphere Research Satellite: A 20 year perspective. *Reviews in Geophysics*, *50*(2), RG2007. https://doi.org/10.1029/2012RG000390

Shepherd, G. G., Thuillier, G., Gault, W. A., Solheim, B. H., Hersom, C., Alunni, J. M., et al. (1993). WINDII—The Wind Imaging Interferometer on the Upper Atmosphere Research Satellite. *Journal of Geophysical Research*, *98*, 10,725–10,750. https://doi.org/10.1029/2012RG000390

Shepherd, M. G. (2016). WINDII observations of thermospheric O(^{1}D) nightglow emission rates, temperature, and wind: 1. The northern hemisphere midnight temperature maximum and the wave 4. *Journal of Geophysical Research: Space Physics*, *121*, 11,450–11,473. https://doi.org/10.1002/2016JA022703

Shepherd, M. G. (2018). Longitudinal and seasonal variations of O(^{1}D) nightglow emission maxima at southern midlatitudes. *Journal of Atmospheric and Solar-Terrestrial Physics*, *167*(107), 123. https://doi.org/10.1016/j.jastp.2-17.11012

Singh, V., Upadhayaya, A. K., & Sunil Krishna, M. V. (2010). Modeling of redline dayglow emission. *IDŐJÁRÁS Quarterly Journal of the Hungarian Meteorological Service*, *114*(3), 217–227.

Thayer, J. P., Crowley, G., Niciejewski, R. J., Killeen, T. L., Buchau, J., & Reinisch, B. W. (1995). Ground-based observations of ion/neutral coupling at Thule and Qânâq, Greenland. *Journal of Geophysical Research*, *100*, 12,189–12,199. https://doi.org/10.1029/95JA00131